Eur. Phys. J. Plus (2019) **134**: 84
DOI 10.1140/epjp/i2019-12485-5

THE EUROPEAN PHYSICAL JOURNAL PLUS

Regular Article

Effect of annealing on phase formation, microstructure and magnetic properties of $MgFe_2O_4$ nanoparticles for hyperthermia*

M. Bououdina[1,a], B. Al-Najar[1], L. Falamarzi[1], J. Judith Vijaya[2], M.N. Shaikh[3], and S. Bellucci[4]

[1] Department of Physics, College of Science, University of Bahrain, PO BOX 32038, Zallaq, Bahrain
[2] Catalysis and Nanomaterials Research Laboratory, Department of Chemistry, Loyola College, Chennai, India
[3] Center of Research Excellence in Nanotechnology (CENT), King Fahd University of Petroleum and Minerals (KFUPM), Saudi Arabia
[4] INFN, Laboratori Nazionali di Frascati, Via E. Fermi 40, 00044, Frascati, Italy

Received: 22 April 2018 / Revised: 14 December 2018
Published online: 1 March 2019

Abstract. In this study the effect of annealing time is confirmed to alter the morphology (shape and size) of magnesium ferrite nanoparticles ($MgFe_2O_4$) synthesized by autoclave route, employing ferric and magnesium nitrate salts as precursors. Annealing was applied at 1000 °C for different durations (2, 30 and 60 h) and Rietveld refinements of X-ray diffraction patterns confirm the formation of pure spinel phase and show that the annealing time has a dominant effect on the crystallite size as it increases from 29 up to 89 nm for 2 to 60 h, respectively. Scanning electron microscopy observations confirm that longer annealing time enhances particle growth, in agreement with the crystallite size obtained by X-ray diffraction analysis. Room temperature magnetic measurements reveal a ferromagnetic behavior with a saturation magnetization (M_s) ranging from 25.84 emu/g for annealing at 2 h and 29.49 emu/g at 60 h. Self-heating characteristics under an alternating current (AC) magnetic field of 17 mT and frequency of 331 kHz were investigated for hyperthermia applications using Magnetherm from Nanotherics. Temperature-time curves indicate that the as-prepared $MgFe_2O_4$ nanoparticles show a considerable heating rate, with a maximum temperature of 48 °C in a very short period of time of 15 min and specific absorption rate (SAR) of 19.23 W/g, when annealed for 60 h.

1 Introduction

Nanoparticles (NPs) have been used widely in modern fields of technology due to their enhanced properties upon their counterpart bulk materials [1]. Their small size, which ranges from few nanometers up to 100 nm, makes them to get through and affect sites of interests [2]. Among NPs, spinel ferrites with the general formula AFe_2O_4 (A = Mn, Co, Ni, Mg, or Zn) are unique due to their tuneable physical and chemical properties according to their nanoscale size [3]. Therefore, they can be synthesized in any specific size and shape depending on their desired application. They also can be produced in many forms, such as thin films [4] and nanopowders [5] that can be shaped as nanofibers [6], nanowires [7], nanospheres [8], and even heteroarchitecture geometry particles [9]. A broad variety of methods are being applied to synthesize Ferrites nanoparticles including ultrasound [10], microwave [11], autoclave [12] and sol-gel [13], etc. Along with the preparation method, annealing temperature and duration have been reported to have a major influence of the microstructure and phase composition of nanoparticles [14] and, hence, to affect the application of nanoparticles too. Applications of spinel ferrites NPs include biosensor [15], photocatalysis [16], drug delivery [17] and hyperthermia [18].

It was shown that under a certain alternating magnetic field a solution of $MgFe_2O_4$ nanopowders, prepared by ultrasonic spray pyrolysis, has its temperature increased by 15 °C [19]. It is also reported that the heating efficiency is influenced by the strength of the applied magnetic field, particle size, concentration and dispersion of the samples [19].

* Focus Point on "Nanotechnology, Nanomaterials and Interfaces" edited by O. Fesenko, L. Yatsenko.

[a] e-mail: mboudina@gmail.com (corresponding author)

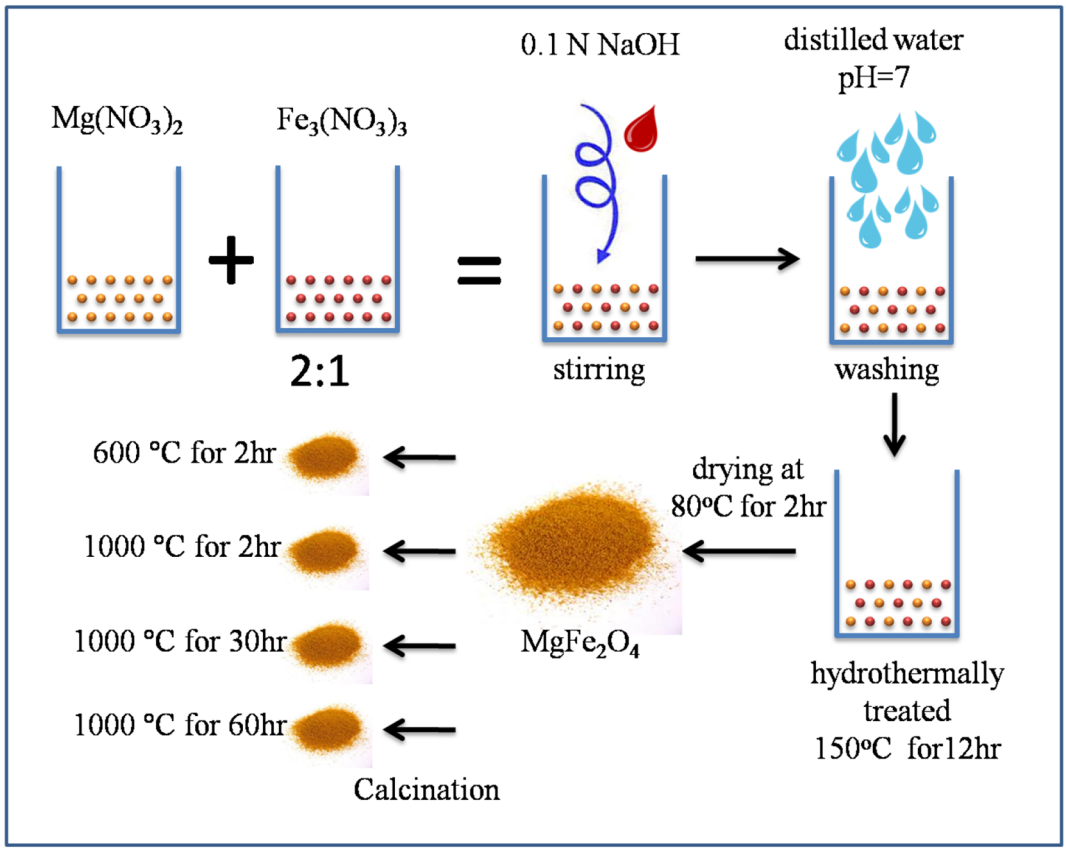

Fig. 1. Autoclave preparation steps of $MgFe_2O_4$ nanopowders annealing at different periods of time.

Such self-heating property in particles can be explained by one or more of the physical mechanisms; eddy current, Neel relaxation, Brownian motion and hysteresis loss [20]. For NPs, the three later mechanisms are more likely to occur, as eddy current is related to bulk materials. This is very essential for hyperthermia application where cancer cells can be successfully destroyed by heating them up to 42 °C for at least 30 min [21]. Spinel ferrites NPs are reported to have a great potential in hyperthermia such as iron oxides (Fe_2O_3) [22] $ZnFe_2O_4$, $CuFe_2O_4$ and $MgFe_2O_4$ [23–25].

In this research work, $MgFe_2O_4$ (the chosen compound contains elements, *i.e.* Mg and Fe, that are biocompatible with human body) NPs were synthesized by autoclave method followed by subsequent annealing at 1000 °C for different duration (2, 30 and 60 h). The aim of this paper is to investigate the effect of particle size in terms of structure, morphology (shape and size), magnetic properties and self-heating characteristics for hyperthermia applications.

2 Experimental part

2.1 Preparation and annealing of $MgFe_2O_4$ nanopowders

Ferric nitrate and magnesium nitrate salts were taken in the molar ratio 2 : 1 and dissolved separately in water. The metal nitrate salts were then mixed together and kept for stirring at room temperature for 3 h. To this solution 0.1 N sodium hydroxide solution was added dropwise while stirring until the precipitate is completely formed. Then the precipitate was washed with distilled water several times until the *p*H reaches 7. The precipitate was hydrothermally treated at 150 °C for 12 h which yielded to $MgFe_2O_4$ powder after drying at 80 °C for 2 h (fig. 1).

An initial XRD pattern of the as-prepared $MgFe_2O_4$ powder (named as $MgFe_2O_4$-AP, annealed at 600 °C for 2 h) showed many peaks diffraction peaks that are very broad (almost typical of an amorphous phase) which was difficult to identify using the database. This indicates that most probably no chemical reaction occurred during the synthesis and that the spinel phase $MgFe_2O_4$ was not fully formed. Therefore, the obtained powder was annealed at 1000 °C using a heating rate of 10 °C/min for three desired periods of time (2, 30 and 60 h, named as $MgFe_2O_4$-T1, $MgFe_2O_4$-T2 and $MgFe_2O_4$-T3, respectively (fig. 1)), in order to form spinel phase $MgFe_2O_4$ and also to examine the effect of different annealing time on structure stability and the evolution of particle morphology (shape and size).

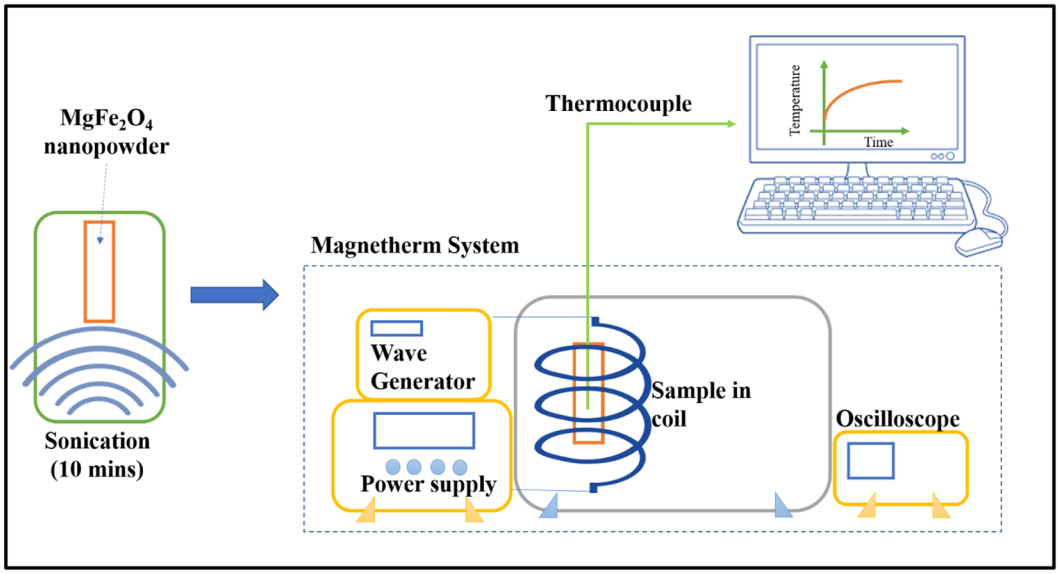

Fig. 2. Schematic diagram showing self-heating properties experiment using a Nanotherics Ltd. magnetherm.

2.2 Characterization of $MgFe_2O_4$ nanopowders

Phase analysis for $MgFe_2O_4$ nanopowders was carried out from X-ray diffraction (XRD) measurement using a high-resolution Rigaku Ultima IV diffractometer equipped with Cu-K α radiation ($\lambda_{k_\alpha} = 1.5418$ Å). Qualitative and quantitative phase analyses were carried out using PDXL program. The refinements were carried out using $MgFe_2O_4$ phase with a spinel cubic crystal structure (space group Fd3m; No. 227), Fe metal with body-centered cubic crystal structure (space group Im-3m, No. 229), and MgO with face centered cubic structure (space group Fm3m No. 225). During refinements, phase composition, lattice parameters and microstructural parameters (crystallite size and microstrain) were refined. The morphology of the nanopowders has been investigated by field emission scanning microscope (FESEM) using JEOL-JSM-7600F equipped with energy dispersive spectroscopy (EDS). Magnetisation-field (M-H) hysteresis loops of the prepared powders were measured at room temperature using PMC MicroMag 3900 model vibrating sample magnetometer (VSM) having a 1 tesla magnet and a sensitivity of 0.5 μemu.

2.3 Self-heating experiment

Self-heating properties for as-prepared and annealed $MgFe_2O_4$ nanopowders, were performed using a Nanotherics Ltd. magnetherm under a magnetic field of 17 mT and a frequency of 331 kHz for two concentrations (5 and 15 mg/mL). Prior to measurements, the powder was dispersed in distilled water by sonication for 15 min. Data acquisition was started at room temperature and a thermocouple was used to measure the temperature change (fig. 2).

3 Results and discussion

3.1 Structural and morphological characteristics

The XRD pattern of the as-prepared $MgFe_2O_4$ powder initially annealed at 600 °C for 2 h shows broad and undefined peaks with low intensity, indicating the presence of an amorphous phase. After further annealing at 1000 °C for different durations (2, 30, 60 h), the XRD patterns shown in fig. 3 demonstrate that with increasing annealing time, the peaks become narrower and their relative intensity increases, indicating the formation of a crystalline phase with an increase in the crystallite size. The observed peaks are indexed within the cubic spinel phase, in agreement with JCPDS card No. 73-1960. The crystallite size and lattice parameter have been calculated using the PDXL program incorporated with the X-ray diffractometer; the results are reported in table 1. The calculated crystallite size ranges from 29.3 to 88.8 nm, which can be attributed to grain growth; annealing provides thermal energy leading to nanoparticles which usually tend to agglomerates and having low surface energy to form large particles. Meanwhile, the lattice parameter is found to decrease slightly as the annealing duration is prolonged, and this can be associated with improved crystallinity and better homogeneity of the bulk powder chemical composition.

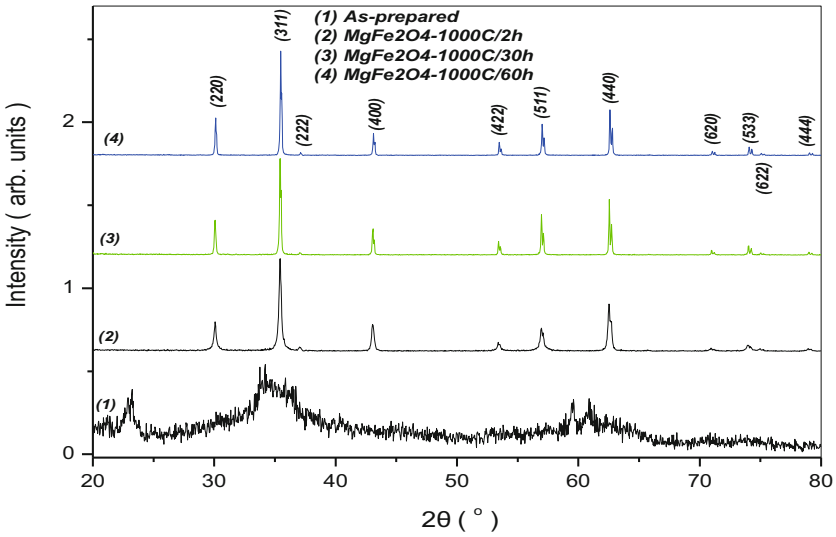

Fig. 3. XRD patterns for $MgFe_2O_4$ samples prepared by autoclave method and annealed at different periods of time.

Table 1. Main characteristics and magnetic properties of $MgFe_2O_4$ samples, obtained from XRD and VSM.

Sample	Lattice parameter a (Å)	Crystallite size CS (nm)	Coercivity H_c (Oe)	Remanence M_r (emu/g)	Saturation Magnetisation M_s (emu/g)
$MgFe_2O_4$-AP	–	–	2.309	1.639	5.399
$MgFe_2O_4$-T1	8.3976	29.3	79.62	3.592	25.84
$MgFe_2O_4$-T2	8.3913	66.8	23.99	3.111	27.39
$MgFe_2O_4$-T3	8.3855	88.8	22.99	3.865	29.49

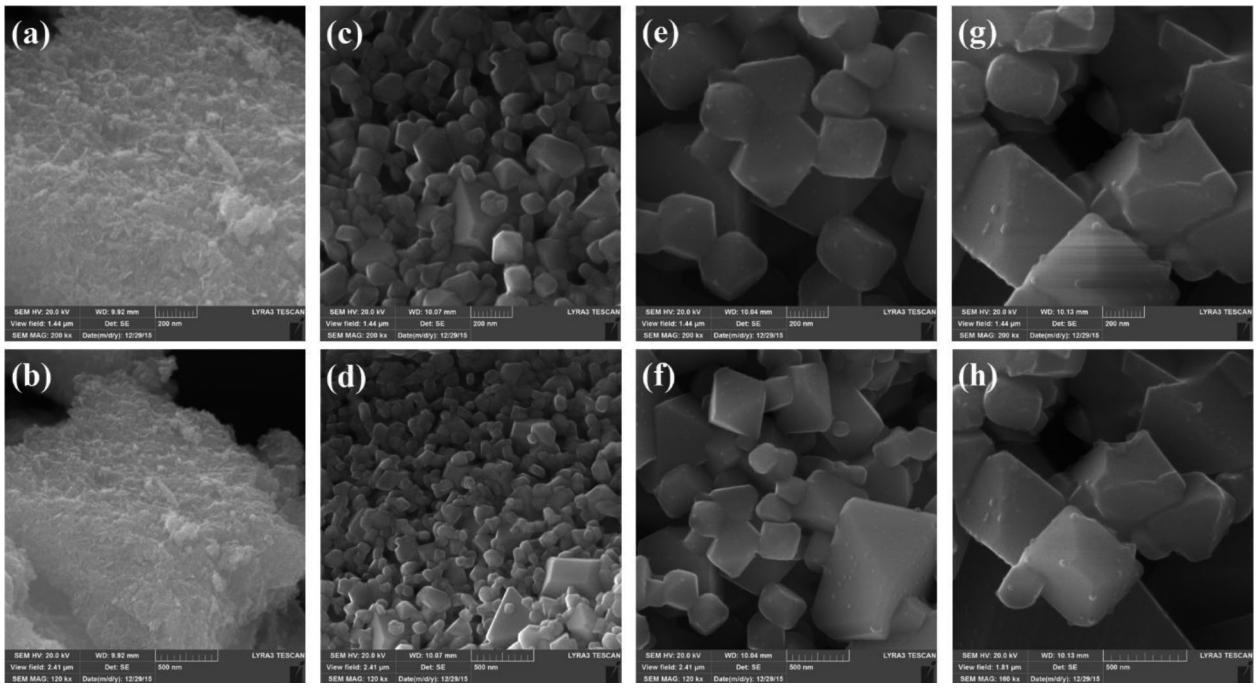

Fig. 4. SEM images for: (a) and (b) $MgFe_2O_4$ prepared by autoclave method and further annealed at 1000 °C; (c) and (d) 2 h; (e) and (f) 30 h; (g) and (h) 60 h.

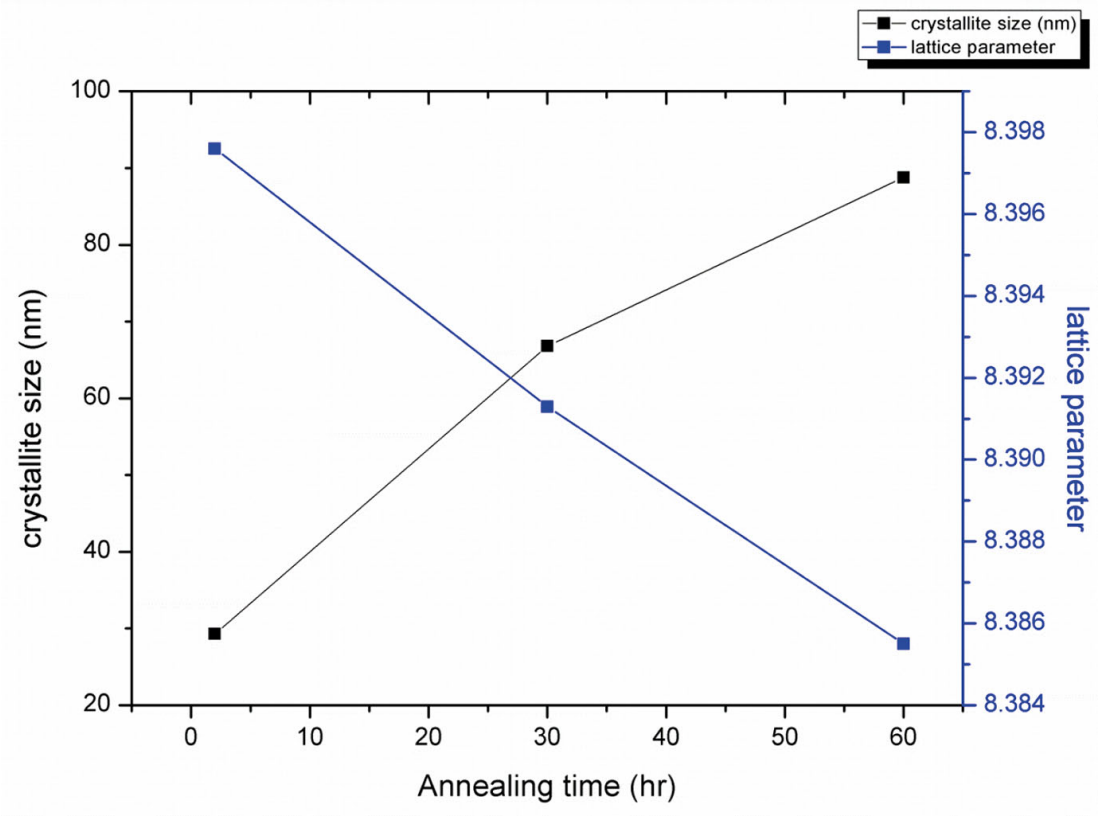

Fig. 5. Relation of crystallite size and lattice parameter with annealing time.

The morphology and chemical composition of the as-prepared and annealed $MgFe_2O_4$ powders were investigated using SEM-EDS. Figures 4(a) and (b) show no defined shape and agglomerated NPs for the as-prepared powder. However, it is obvious from SEM images (figs. 4(c) to (g)) that annealing has a significant influence on the particle morphology and size of the as-prepared $MgFe_2O_4$ powder, as cube grains with smooth facets at the nanoscale are clearly formed. Furthermore, grain growth can be noticed with increasing annealing time from 2 to 60 h, which can be considered as an evidence of the increase in particle size in agreement with the values of crystallite size obtained from XRD analysis (table 1). Also, the grains become smoother with less agglomeration. It is reported that the annealing time will cause a considerable grain growth especially at higher temperatures [26–28]. This could occur as a result of the associated decrease in micro-hardness [28]. Also, as can be seen from fig. 5, the rate of grain growth decreases for larger grains. This can be explained by the reduction in the grain boundary total energy [28]. This could be associated with the lattice parameter that decreases with larger grain size (table 1). It is essential to mention here that many factors influence the relation between grain growth and temperature and therefore, further study of grain growth kinetics is essential to investigate this relation.

Figure 6, shows typical EDS spectra of a selected region of the as-prepared and annealed $MgFe_2O_4$ nanopowders. It can be seen that only peaks related to Mg, Fe and O elements are observed, which confirms the purity of the prepared powders. In addition, from table 2, it can be noticed that the atomic chemical composition is very close to the stiochiometric $MgFe_2O_4$.

3.2 Magnetic properties

The magnetization-field (M-H) curves of as-prepared and annealed $MgFe_2O_4$ nanopowders obtained from room temperature VSM measurements are shown in fig. 7. It is clear that the reference sample shows superparamagnetic behavior. A dramatic change in magnetization was observed with further annealing at 1000 °C for 2, 30 and 60 h; as room temperature ferromagnetism (RTFM) can be confirmed. A small paramagnetic component was removed to obtain the correct values of saturation magnetization (M_s) reported in table 1. The curves are typical for a soft magnetic material and indicate ferromagnetic order with a hysteresis loop in the field range of ±5000 Oe, while outside this range the magnetisation increases with increasing the applied magnetic field and tends to saturate in the investigated field range (±10 kOe). According to the results (table 1), M_s has a major increase from 5.4 emu/g for the reference

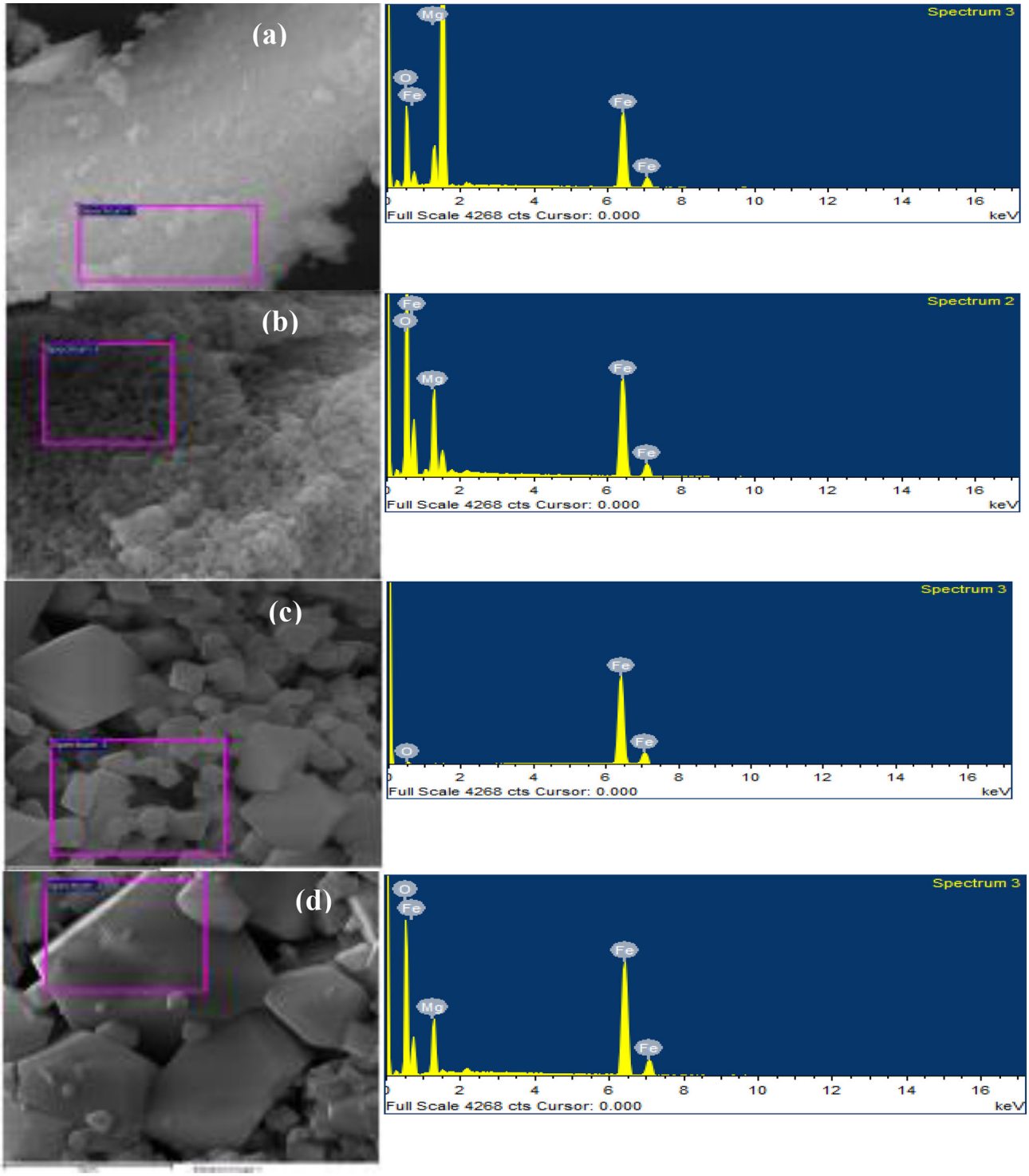

Fig. 6. EDS analysis for: (a) $MgFe_2O_4$ nanopowders prepared by autoclave method and further annealed at 1000 °C; for (b) 2 h; (c) 30 h; (d) 60 h.

sample up to 5 times, reaching 25.8 emu/g after at 1000 °C for 2 h, which indicates the strong influence of annealing time and temperature on the magnetic behaviour of $MgFe_2O_4$ due to the major changes in particle morphology/size and the formation of crystalline phase as confirmed by XRD and SEM-EDS analyses. With longer annealing duration (30 and 60 h), M_s gradually increases due to the minor effect of longer annealing time on phase formation (single phase if already formed for only 2 h) and chemical composition homogeneity.

Table 2. Atomic chemical composition for prepared $MgFe_2O_4$ samples with further annealing obtained by EDS.

Sample	Mg	O	Fe
$MgFe_2O_4$-AP	19.5	56.37	24.48
$MgFe_2O_4$-T1	14.97	69.48	15.55
$MgFe_2O_4$-T2	1.96	6.53	91.52
$MgFe_2O_4$-T3	13.7	63.48	22.82

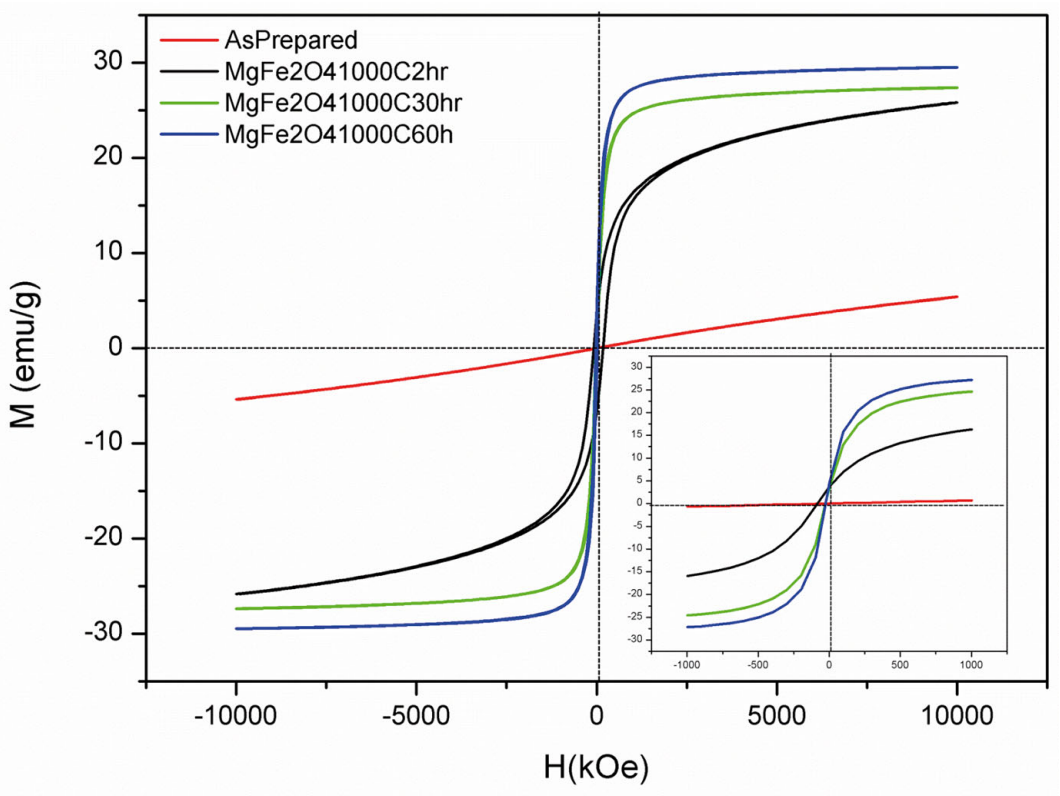

Fig. 7. Hysteresis loops for $MgFe_2O_4$ nanopowders prepared by autoclave and further annealed at different durations. (Reference $MgFe_2O_4$ is the as-prepared sample).

3.3 Self-heating characteristics

Heating curves of the synthesized $MgFe_2O_4$ samples for different concentrations (10 and 15 mg/mL), under frequency of 331 kHz and magnetic field of 17 mT are shown in fig. 8. It can be seen that all heating curves has two clear slopes, a sharp temperature increase occurring during the first 1-2 minutes then it continuous to increase gradually. This behavior was already observed in Zn-doped $MgFe_2O_4$ samples prepared by sol-gel method [29] and also in other ferrite systems [30,31]. The initial slope is due to the alignment of particles under the AC magnetic field [29], while the second slope was related to the hysteresis loss because of the ferromagnetic nature of the samples. There are three mechanisms related to the heat generation in nanoparticles, namely: i) Hysteresis loss; ii) Brownian relaxation; and iii) Neel relaxation. Herein, it is important to highlight that none of the above mentioned mechanism can be the only origin of heat generation; it is more likely a combination of the three is more favorable. Moreover, it can clearly be noticed that the heating rate of the samples has obviously increased with increasing annealing time and concentration, as $MgFe_2O_4$-T3 with 15 mg/mL has the maximum heating rate as well as the maximum temperature, reaching 46 °C in 15 min. More interestingly, after reaching a temperature of 42 °C, it is maintained for almost 10 mins which is very essential and can be considered as an ideal condition for a successful hyperthermia treatment [23]. Herein, it is very important to mention that our starting temperature is room temperature and if the human body normal temperature 37 °C is considered, then reaching the critical temperature will be faster. Hence, considering the slope by calculating the SAR value is one of the reliable ways to assess the efficiency of MNPs for hyperthermia application.

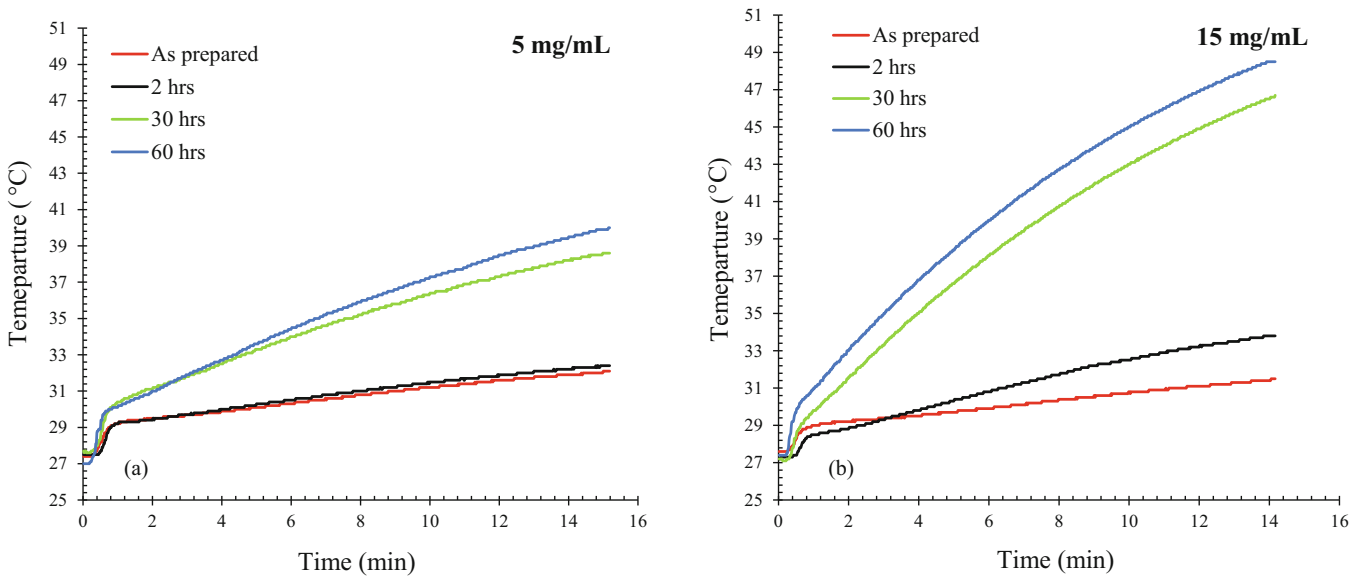

Fig. 8. Heating curves for $MgFe_2O_4$ nanopowders prepared by autoclave and further annealed at different durations at concentrations of (a) 5 or 10 mg/mL and (b) 15 mg/mL.

Table 3. Self heating characteristics and SAR values for prepared $MgFe_2O_4$.

Samples	Concentration (mg/mL)	Initial linear slope (°C/s)	SAR (W/g)	Maximum temperature (°C)	Crystallite size (nm)	Hysteresis loss $H_c \times M_r$ (Oe.emu/g)
$MgFe_2O_4$-AP	10	0.013	10.87	40	–	3.78
$MgFe_2O_4$-T1		0.014	11.70	39	29.3	285.99
$MgFe_2O_4$-T2		0.025	20.90	32	66.8	74.63
$MgFe_2O_4$-T3		0.023	19.23	32	88.8	88.856
$MgFe_2O_4$-AP	15	0.01	2.79	32	–	3.78
$MgFe_2O_4$-T1		0.015	4.18	34	29.3	285.99
$MgFe_2O_4$-T2		0.035	9.75	46	66.8	74.63
$MgFe_2O_4$-T3		0.04	11.15	48	88.8	88.856

The specific absorption rate (SAR) was calculated as follows:

$$SAR = C * \frac{\Delta T}{\Delta t} * \frac{m_{\text{sample}}}{m_{\text{water}}}, \quad [30]$$

where C is the specific heat capacity of water (4.180 (J/(g · C))), $\Delta T/\Delta t$ is the initial slope of the temperature change with time for the first 2 minutes and m is the total mass of the sample and water. Surprisingly, from table 3, it can be noticed that the solutions of less $MgFe_2O_4$ concentration (10 mg/mL) have higher SAR values: $MgFe_2O_4$-T3 has a higher SAR value at 10 mg/mL (19.23 W/g) than 15 mg/mL (11.15 W/g). This can be explained by the very slight difference obtained for the initial slopes (0.017 C/s), while a considerable concentration difference is there (10 mg/mL). In addition, SAR value can be also related to the crystallite (particle) size and crystallinity; it increases with increasing crystallite size from 29.3 to 66.8 nm. However, for much larger crystallite size of 88.8 nm, the SAR value does not change that much, which means the existence of an optimum value of crystallite size where self-heating reach a steady state (equilibrium). On the other hand, for other reported ferrite systems [29,31,32], samples with smaller crystallite size ranging from 9 to 20 nm, showed similar self-heating characteristics compared to $MgFe_2O_4$ nanopowders obtained in this study, see table 4.

Table 4. Comparison between the obtained SAR values for $MgFe_2O_4$ samples and other ferrite systems reported in the literature.

Ferrite system	Synthesis method	Concentration (mg/mL)	Frequency (kHz)	Magnetic field (mT)	SAR (W/g)	Staring temperature	Time needed to reach 42 °C (min)	Crystallite size (nm)	References
$MgFe_2O_4$-T3	Autoclave	10	331	17	19.23	27	18	88.8	This work
$MgFe_2O_4$-T3	Autoclave	15	331	17	11.15	27	7	88.8	This work
$Zn_{0.5}Ca_{0.5}Fe_2O_4$	Sol-gel	10	354	12.8	14.8	28	Not reached in 15 min	14	[31]
$Mg_{0.9}Zn_{0.1}Fe_2O_4$	Sol-gel	10	354	12.8	10.29	36.5	Not reached in 10 min	17	[25]
$Mg_{0.7}Zn_{0.3}Fe_2O_4$	Sol-gel	10	354	12.8	18.73	36.5	6 min	17	[25]
$MgFe_2O_4$	Sol-gel	25	198	11.6	19	20	0.5 min	9.2	[32]

In order to have further assessment of the efficiency of our prepared nanopowders for hyperthermia treatment, self-heating characteristics were compared to some results reported in the literature for similar ferrite systems, see table 4. As reaching 42 °C is a critical point in hyperthermia treatment, where cancer cells can be destroyed, the time needed to reach this specific temperature was one of the comparison parameter as well as the starting temperature. The sol-gel $Mg_{0.7}Zn_{0.3}Fe_2O_4$ solution of (10 mg/mL) reached the critical temperature in 6 mins [28], which is a very similar time to that of $MgFe_2O_4$-T3 (15 mg/mL); however, if the starting temperature is taken into account, the latter could be more efficient for hyperthermia treatment. Another study on $MgFe_2O_4$ powders showed a very fast temperature rise (from 20 to 42 °C in 0.5 min), however, their calculated SAR values are almost the same as for $MgFe_2O_4$-T3. Therefore, the maximum temperature and the time needed to reach the critical temperature of 42 °C, in addition to SAR value, can be considered the main factors to be taken into consideration during the development of new nanomaterials for hyperthermia and for comparison.

Both our prepared $MgFe_2O_4$-T2 and $MgFe_2O_4$-T3 nanopowders have shown a promising SAR value at low concentration (10 mg/mL) while reaching the critical temperature in a relatively short duration of only 7 min in higher concentrations (15 mg/mL) taking into consideration the experimental conditions (magnetic field and frequency) compared to the values reported in table 4, and hence have great potential for hyperthermia application.

4 Conclusion

In this paper, $MgFe_2O_4$ nanopowders were prepared through autoclave route with further annealing at different durations that evidently changed their morphology and magnetic properties. Annealing time was found to have a large influence on the crystal growth. Further investigation of grain growth kinetics could give a clearer explanation about this relation. The obvious obtained crystal growth and higher saturation magnetization accordingly altered the self-heating characteristics of the powders and the sample with longer annealing time showed higher temperature raise reaching 48 °C. Other samples did not reach a very high temperature but maintain a good temperature raise at lower concentration and so on; a high SAR value of 20.9 W/g is obtained. Considering two different assessments of self-heating, it can be concluded that the as-prepared $MgFe_2O_4$ nanopowders possess a high potential to be applied efficiently in hyperthermia application. Meanwhile, a better understanding of the origin and the effects of such temperature raise need further studies as self-heating properties have been found to be influenced by several factors including concentration of nanoparticles and frequency of the applied magnetic field. Further studies on magnetic properties as well as the behavior of these prepared nanopowders in other mediums such as cell culture or animal tissue would allow a clearer prospective to a hyperthermia treatment using magnetic nanoparticles.

MB would like to thank the Deanship of Research at the University of Bahrain for the financial support of this research project.

References

1. R.M. Patil, N.D. Thorat, P.B. Shete, S.V. Otari, B.M. Tiwale, S.H. Pawar, Mater. Sci. Eng. C **59**, 702 (2016).
2. A.U. Rashid, P. Southern, J.A. Darr, S. Awan, S. Manzoor, J. Magn. & Magn. Mater. **344**, 134 (2013).
3. J. Huanga, M. Chena, W. Kuoa, Y. Suna, F. Lin, Ceram. Int. **41**, 2399 (2015).
4. M. Mishra, A. Roy, A. Garg, R. Gupta, S. Mukherjee, J. Alloys Compd. **721**, 593 (2017).
5. L. Li, X. Zhong, R. Wang, X. Tu, J. Magn. & Magn. Mater. **435**, 58 (2017).
6. A.M. EL-Rafei, A.S. El-Kalliny, T.A. Gad-Allah, J. Magn. & Magn. Mater. **428**, 92 (2017).
7. F. Ebrahimi, S.R. Bakhshi, F. Ashrafizadeh, A. Ghasemi, Mater. Res. Bull. **76**, 240 (2016).
8. Y. Bi, Y. Ren, F. Bi, T. He, J. Alloys Compd. **646**, 827 (2015).
9. Z. Song, Y. He, Appl. Surf. Sci. **420**, 911 (2017).
10. Inukai, N. Sakamoto, H. Aono, O. Sakurai, K. Shinozaki, H. Suzuki, N. Wakiya, J. Magn. & Magn. Mater. **323**, 965 (2011).
11. M. Venkatesh, G. Suresh Kumar, S. Viji, S. Karthi, E.K. Girija, Mod. Electron. Mater. **2**, 74 (2016).
12. M. Ristic, S. Krehula, M. Reissner, M. Jean, S. Musić, J. Mol. Struct. **1140**, 32 (2017).
13. R.R. Bhosale, A. Kumar, F. AlMomani, I. Alxneit, Ceram. Int. **42**, 2431 (2016).
14. L.L. Mguni, M. Mukenga, K. Jalama, R. Meijboom, Catal. Commun. **34**, 52 (2013).
15. F.S. Yardımcı, M. Şenel, A. Baykal, Mater. Sci. Eng. C **32**, 269 (2012).
16. M. Sundararajan, L. John Kennedy, P. Nithya, J. Judith Vijaya, M. Bououdina, J. Phys. Chem. Solids **108**, 61 (2017).
17. C.S.S.R. Kumar, F. Mohammad, Adv. Drug Deliv. Rev. **63**, 789 (2011).
18. O.M. Lemine, K. Omri, M. Iglesias, V. Velasco, P. Crespo, P. de la Presa, L. El Mir, Houcine Bouzid, A. Yousif, Ali Al-Hajry, J. Alloys Compd. **607**, 125 (2014).
19. H. Das, N. Sakamoto, H. Aono, K. Shinozaki, H. Suzuki, N. Wakiy, J. Magn. & Magn. Mater. **392**, 91 (2015).
20. A.E. Deatsch, B.A. Evans, J. Magn. & Magn. Mater. **354**, 163 (2014).
21. Q.A. Pankhurst, J. Connolly, S.K. Jones, J. Dobson, J. Phys. D **36**, R167 (2003).
22. B.B. Lahiri, T. Muthukumaran, J. Philip, J. Magn. & Magn. Mater. **407**, 101 (2016).
23. H. Hirazawa, H. Aono, T. Naohara, T. Maehara, M. Sato, Y. Watanabe, J. Magn. & Magn. Mater. **323**, 675 (2011).
24. V.M. Khot, A.B. Salunkhe, N.D. Thorat, M.R. Phadatare, S.H. Pawar, J. Magn. & Magn. Mater. **332**, 48 (2013).
25. P. Yajaira Reyes-Rodrígueza, D. Alicia Cortés-Hernández *et al.*, J. Magn. & Magn. Mater. **427**, 268 (2017).
26. R. Alizadeh, R. Mahmudi, A.H.W. Ngan, T.G. Langdon, J. Mater. Sci. **50**, 4940 (2015).
27. M.R. Akbarpour, H.S. Kim, Mater. Design **83**, 644 (2015).
28. M.R. Akbarpour, M. Farvizi, H.S. Kim, Mater. Design **119**, 311 (2017).
29. T. Zargar, A. Kermanpur, Ceram. Int. **43**, 5794 (2017).
30. A. Doaga, A.M. Cojocariu *et al.*, Mater. Chem. Phys. **143**, 305 (2013).
31. R. Argentina Jasso-Terán, D. Alicia Cortés-Hernández *et al.*, J. Magn. & Magn. Mater. **427**, 241 (2017).
32. H.M. El-Sayed, I.A. Ali, A. Azzam, A.A. Sattar, J. Magn. & Magn. Mater. **424**, 226 (2017).